A mathematical model of mitochondrial calcium-phosphate dissolution as a mechanism for persistent post-CSD vasoconstriction

Shixin Xu[1,2], Joshua C. Chang[3,*], Carson C. Chow[3], and Huaxiong Huang[4,2,*]

[1]Duke Kunshan University, 8 Duke Ave., Suzhou, China, 215316
[2]Centre for Quantitative Analysis and Modeling (CQAM), The Fields Institute for Research in Mathematical Sciences, 222 College Street, Toronto, Ontario, M5T 3J1, Canada
[3]Laboratory of Biological Modeling, NIDDK, National Institutes of Health, Bethesda MD, USA
[4]Department of Mathematics and Statistics, York University, Toronto, ON, M3J 1P3, Canada
[*]Corresponding authors: joshchang@ucla.edu, huaxiong.huang@gmail.com

August 12, 2019

Abstract

Cortical spreading depolarization (CSD) is the propagation of a relatively slow wave in cortical brain tissue that is linked to a number of pathological conditions such as stroke and migraine. Most of the existing literature investigates the dynamics of short term phenomena such as the depolarization and repolarization of membrane potentials or large ion shifts. Here, we focus on the clinically-relevant hour-long state of neurovascular malfunction in the wake of CSDs. This dysfunctional state involves widespread vasoconstriction and a general disruption of neurovascular coupling. We demonstrate, using a mathematical model, that dissolution of calcium that has aggregated within the mitochondria of vascular smooth muscle cells can drive an hour-long disruption. We determine the rate of calcium clearance as well as the dynamical implications on overall blood flow. Based on reaction stoichiometry, we quantify a possible impact of calcium phosphate dissolution on the maintenance of F_0F_1-ATP synthase activity.

1 Introduction

Cortical spreading depolarization (CSD), also known as cortical spreading depression [46, 50, 52, 15, 9], is a slow-moving propagating wave in cortical gray matter tissue. Its presence is widespread in distressed states including traumatic brain injury, stroke, and migraine with aura [45, 23]. CSD presents at several timescales. The two-minute timescale of changes occurring as the wave passes is fairly well-studied, as is the transient quiescence of neuronal activity in its wake [58]. However, an hour-long period characterized by persistent vasoconstriction [44] and derangement in neurovascular coupling [13] (NVC) remains relatively enigmatic. Neurovascular coupling refers to the dynamical matching of cerebral blood flow to changes in metabolic need induced by neuronal activity [27, 21]. This longer timescale is clinically relevant, for instance in concussion syndrome after traumatic brain injury [8].

Here, we advance a mathematical model for the persistent vasoconstriction based on the following experimental observations: 1) During the acute phase of CSD, extracellular ionic calcium drops by 90% while intracellular calcium elevates to super-physiological concentrations [28]. 2) Vasoconstriction is ultimately controlled by calcium dynamics in vascular smooth muscle cells [21]. 3) Blockage of mitochondrial permeability transition pore (mPTP) formation in the acute phase of CSD prevents the persistent vascular phenotype [54]. The mPTP may be allowing large amounts of calcium to enter mitochondria. 4) Mitochondria are limitless reservoirs for calcium absorption through precipitation of calcium phosphate species [11] – in vascular smooth muscle they may act as a source for calcium. 5) Supersatured solutions balance aggregation and dissolution to settle at a lower thermodynamically stable concentration [63, 22] that is lower than the total concentration. 6) The rates of exchange mechanisms depend on the active soluble concentration of calcium rather than the total concentration.

Overall, we consider the implications of the formation of clusters - with their implied steady state elevation of mitochondria calcium - on cytosolic calcium dynamics within vascular smooth muscle cells. In this model, the saturation concentration rather than the total concentration of calcium in the matrix determines the exchange rate between mitochondria and the cytosol. Using this model, we demonstrate that it can account for the observed

hour-long timescales while mimicking the macroscopic phenotype of the pial artery diameter of Figure 4A of Chang et al. [13].

1.1 CSD: Setting the stage

Mechanistically, CSD is a self-propagating metabolic wave that involves all electrically polar cells in the affected tissue - neurons, glia, and vascular cells. Although synaptic vesicle release occurs during CSD, the primary driver of CSD seems to be extra-synaptic activity through what has been termed "volume-transmission," where CSD is best-described as a reaction-diffusion phenomenon [50]. In CSD, widespread cellular depolarization occurs in the presence of focally large extracellular concentrations of potassium and excitatory neurotransmitters such as glutamate at the wavefront [24, 73]. In turn, this depolarization induces the release of more potassium and glutamate, sustaining wave propagation. The vasculature is an active participant. There is evidence that vascular cells conduct the wave along their major axes [10, 41]. Besides conducting the wave, arteries in the brain respond to the elevated potassium by constricting [17], although the change in oxygen supply does not itself appear to have much effect on the properties of the propagating wavefront [14].

The recovery of the tissue following a CSD is biphasic. The first phase corresponds to the recovery at the acute wavefront and lasts approximately two minutes from an initial elevation of extracellular potassium and glutamate to a general quiescence of activity. At the end of this phase, extracellular potassium, sodium, and glutamate recover to near their pre-CSD levels. The second phase involves the recovery from tissue-scale derangements. Several minutes after the end of the acute phase, cerebral tissue undergoes changes [2]. The cerebral vasculature exhibits dysregulation in NVC [53, 13]. Beyond the mismatch of blood flow to neuronal metabolic need, overall blood flow is reduced [43] as cerebral vasculature notably constricts relative to baseline. Neural-cognitive impairment in the form of decreased plasticity is also present [64]. The recovery from this state occurs on the timescale of an hour [13].

In the acute phase, extracellular calcium concentration drops from a baseline of over 1 mM to under 0.1 mM [32]. The actual net movement of calcium is even more drastic when accounting for the fact that the extracellular space shrinks in half due to the increase in cellular volume from the increased osmotic pressure [31]. These two factors combined imply that approximately 95% of the initial extracellular calcium transfers into cells during the acute phase.

Lacking vascular smooth muscle calcium measurements of calcium dynamics during CSD, we rely on neuronal measurements, where cytosolic calcium elevation has been observed [24]. In experiments in the absence of external calcium, there is no elevation of neuronal intracellular calcium [3], suggesting an extracellular source of calcium. We know from the fact that the vasculature constricts in the acute phase that cytosolic calcium is elevated throughout its duration. Some of this calcium is presumably buffered within mitochondria. Under normal circumstances, the amount of calcium entering the matrix is limited by the uptake of the mitochondrial calcium uniporter (MCU) [69]. However, in CSD, mitochondrial depolarization [62] induces the formation of the mitochondrial permeability transition pore (mPTP), a non-specific pore across the mitochondrial membrane. Blockage of mPTP formation has been shown to prevent the second phase [54]. In typical settings, formation of this pore implies the exit of calcium out from an overloaded mitochondria into the cytosol [4]. CSD is not a typical situation. In CSD, this pore forms while cytosolic calcium is elevated within the cytosol. Hence, the mPTP provides a mechanism for large-scale calcium entry into the matrix.

As opposed to the acute stage [25], vasoconstriction in the second phase is not due to extracellular potassium [13], which would suggest an extracellular voltage-dependent calcium source for inducing vasoconstriction. In this manuscript, we propose a vasogenic source of vasoconstrictive free calcium. Through mathematical modeling, we examine the hypothesis that slow calcium release from mitochondrial calcium stores of vascular origin can account for the behavior seen in this longer phase of recovery.

1.2 Mitochondrial calcium uptake

In CSD, cells in the gray matter absorb calcium. Vascular smooth muscles cells, are known to be adept at absorbing calcium, with excess calcium mineralizing in the mitochondrial matrix [70]. Mitochondria are calcium buffers of last resort. The primary calcium uptake mechanisms for mitochondria are the MCU and the reversible mitochondrial sodium-calcium exchanger (NCLX). In normal physiological states, mitochondria are likely not important buffers of calcium [69]. The endoplasmic (sarcoplasmic in muscle) reticulum (ER) offers a stronger but limited basin for calcium sequestration. However, mitochondria are the dominant mechanism for calcium sequestration in highly distressed cell states due to their virtually limitless capacity for calcium buffering [11]. The buffering capacity is not due to presence of binding proteins as in other cell compartments. Rather, this capacity arises from interactions between ionic calcium, inorganic phosphate, and protons that result in nucleation and growth of calcium orthophosphate

clusters [68, 22]. Here, nucleation refers to the physical process by which ordered states like clusters arise from less-ordered states like supersaturated solutions, where supersaturation is a state where solutes are crowded in solution past a critical concentration where it is thermodynamically favorable to cluster. A limited mechanism for inhibiting nucleation exists within mitochondria. Inorganic phosphate exists both in its free monomeric forms ($PO_4{}^{3-} \rightleftharpoons HPO_4{}^{2-} \rightleftharpoons H_2PO_4{}^{-} \rightleftharpoons H_3PO_4$) and in polymeric forms as inorganic polyphosphate (polyP [42]) molecules, held together by the same phosphoanhydride bonds that endow ATP with high chemical potential energy. PolyP is thought to inhibit the formation of clusters [59], by binding to precursors called prenucleation clusters [26, 20].

1.3 Calcium phosphate nucleation and dissolution

In solutions, solvation describes the complicated interactions between a solvent and solute particles. The observed dynamics result as an interplay between two competing drives - solute-solvent interactions, and solute-solute interactions. A solution is said to be at saturation when these drives are balanced, and at supersaturation when solute-solute interactions dominate. When there is an excess of solute relative to the saturation point, precipitation is thermodynamically favored. However, precipitation is often limited by kinetic considerations. The rate-limiting step in this process is nucleation, which depends on the chemical properties of the solution.

The chemical interactions between calcium, inorganic phosphate, and other salts in aqueous solution are complex [16, 68, 22, 72]. When calcium and phosphate are at sufficiently high concentrations, they co-aggregate to form complexes of varying stoichiometry [56], first as prenucleation clusters [29], and then as stable nuclei. Prenucleation clusters offer a quicker path to particle condensation than predicted according to nucleation kinetics. For calcium phosphate in the process of condensation, protons are liberated into the solution decreasing the pH [22].

Biological solutions exist in a baseline state of supersaturated calcium and phosphate, maintaining this state actively through the action of nucleation inhibitors. These inhibitors prevent runaway calcification from occurring. The main inhibitor of calcium phosphate nucleation in extracellular bodily fluids is fetuin-A [35, 34, 38], which has strong affinity for prenucleation clusters, thereby exponentially increasing the concentration of calcium that is able to exist stably in solution [12]. In the presence of nuclei, a reduction of free calcium or phosphate concentration below the thermodynamic saturation point results in dissolution which replenishes the free concentration. Elevations result in aggregation which reduces the free concentration. Hence, the saturation point is a thermodynamically stable steady state.

We assume that the mitochondrial matrix exists at quasi-steady equilibrium at saturation and examine the implications of this persistent calcium elevation on cellular calcium dynamics. To set the stage for this state, we assume that large quantities of calcium have entered the mitochondria during the acute phase of CSD, through the mPTP. After closure of the mPTP and commencement of the aggregation process, we assume that the mitochondria is able to return to a stable baseline pH, where the usual exchange mechanisms act to expel the excess calcium stores.

2 Mathematical Model

The chief objective of our model is to understand the dynamics of free ionic calcium in the cytosol as calcium leaking from mitochondrial stores interact with the various cellular mechanisms for calcium homeostasis.

We denote concentrations using square brackets (e.g. $[Ca^{2+}]$ corresponds to the concentration of free ionic calcium), generally parameterized in units of millimolar (μ-moles per liter). The concentrations are specific to subcellular or extracellular compartments – we keep track of these using subscripts. The compartments modeled are the extracellular space (ecs), the cytosol (cyt), the mitochondrial matrix (mit), and the endo(sarco)plasmic reticulum (er). Concentration fluxes (of calcium) between the compartments are denoted by J and assumed to be oriented so that positive J is relative to positive changes in cytosolic calcium concentration. Additionally, all J fluxes are scaled to the cytosolic volume.

The intracellular compartments have volumes denoted by V_{cyt}, V_{mit}, V_{er}. Note that these volumes are overall volumes within a single cell - the mitochondrial volume scales with the number of total mitochondria. From these volumes arise the volume ratios

$$r_{\text{er}}^{\text{cyt}} = \frac{V_{\text{cyt}}}{V_{\text{er}}} = 10, \quad r_{\text{mit}}^{\text{cyt}} = \frac{V_{\text{cyt}}}{V_{\text{mit}}} = 13.6, \tag{1}$$

where the cytosolic volume is assumed to be 0.7 pL and the mitochondrial volume ratio is taken from Wacquier et al. [66]. We assume that calcium is well-mixed within each compartment, denoting the compartmental concentrations as $[Ca^{2+}]_{\text{cyt}}$, $[Ca^{2+}]_{\text{mit}}$ and $[Ca^{2+}]_{\text{er}}$ accordingly.

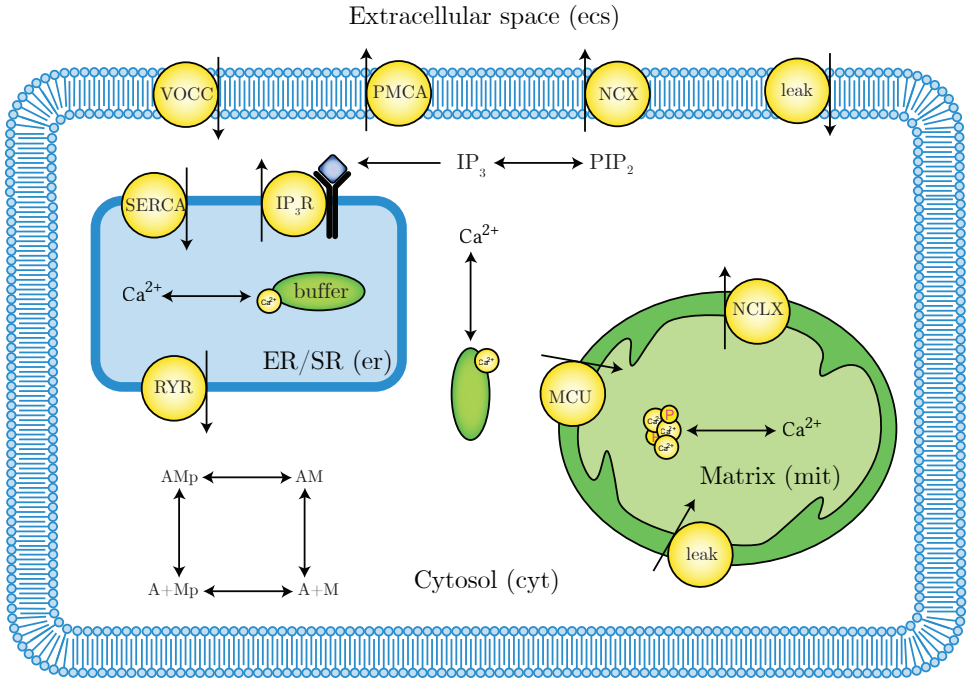

Figure 1: **Model schematic** showing compartments, calcium exchanges, and other reactions specifically considered. Note that only calcium ions are considered in our model so we ignore counter-transporters such as sodium. Most of the exchange mechanisms are bidirectional – direction that is relevant to the scope of our model is depicted.

2.1 Cytosol

The concentration of calcium in the cytosol obeys mass balance through the ordinary differential equation

$$\frac{\mathrm{d}[\mathrm{Ca}^{2+}]_{\mathrm{cyt}}}{\mathrm{d}t} = \frac{1}{b_{\mathrm{cyt}}}\left(J_{\mathrm{er}\to\mathrm{cyt}} + J_{\mathrm{mit}\to\mathrm{cyt}} + J_{\mathrm{ecs}\to\mathrm{cyt}} + J_{\mathrm{cyt}\to\mathrm{cyt}}\right). \tag{2}$$

The flux terms account for exchange between the cytosol and other compartments, as well as reactions within the cytosol. The term in the denominator of Eq. 2 models calcium buffering and is given by

$$b_{\mathrm{cyt}} = 1 + \frac{K_{\mathrm{CaM}}[\mathrm{CaM}]_{\mathrm{cyt}}}{\left(K_{\mathrm{CaM}} + [\mathrm{Ca}^{2+}]_{\mathrm{cyt}}\right)^2} + \frac{K_{\mathrm{B}}[\mathrm{B}]_{\mathrm{cyt}}}{\left(K_{\mathrm{B}} + [\mathrm{Ca}^{2+}]_{\mathrm{cyt}}\right)^2}. \tag{3}$$

It is due to the rapid buffer approximation (RBA) [67], a form of the total quasi-steady-state approximation [7], which accounts for the effects of binding proteins (parameters given in Table. 1). Note that we explicitly distinguish between (active) free ionic calcium and (inactive) bound calcium in our model. Consistent with this approximation, the total (free + bound) concentration of calcium follows

$$[\mathrm{Ca}^{2+}]_{\mathrm{cyt,tot}} = [\mathrm{Ca}^{2+}]_{\mathrm{cyt}}\left(1 + \frac{K_{\mathrm{CaM}}[\mathrm{CaM}]_{\mathrm{cyt}}}{K_{\mathrm{CaM}} + [\mathrm{Ca}^{2+}]_{\mathrm{cyt}}} + \frac{K_{\mathrm{B}}[\mathrm{B}]_{\mathrm{cyt}}}{K_{\mathrm{B}} + [\mathrm{Ca}^{2+}]_{\mathrm{cyt}}}\right). \tag{4}$$

where all quantities are fixed and listed in Table 1.

The primary phenotype of interest that is caused by perturbed calcium dynamics is vasoconstriction. We model vasoconstriction and dilation indirectly through a four-state model of calcium-dependent actin/myosin dynamics

$$\begin{aligned}
\mathrm{M} &= 1 - \mathrm{Mp} - \mathrm{AMp} - \mathrm{AM} \\
\frac{\mathrm{dMp}}{\mathrm{d}t} &= K_4 \times \mathrm{AM}p + K_1 \times \mathrm{M} - (K_2 + K_3) \times \mathrm{Mp} \\
\frac{\mathrm{dAMp}}{\mathrm{d}t} &= K_3 \times \mathrm{M}p + K_6 \times \mathrm{AM} - (K_4 + K_5) \times \mathrm{AMp} \\
\frac{\mathrm{dAM}}{\mathrm{d}t} &= K_5 \times \mathrm{AMp} - (K_7 + K_6) \times \mathrm{AM},
\end{aligned} \tag{5}$$

	Parameter	Value	Notes
Buffer	K_{CaM}	0.260 μM	Rescaled from Johny et al. [39] to yield a baseline buffering ratio of 1%, consistent with Wacquier et al. [65]
	$[\mathrm{CaM}]_{\mathrm{cyt}}$	30 μM	
	K_{B}	0.530 μM	
	$[\mathrm{B}]_{\mathrm{cyt}}$	30 μM	
	[Myo]	10 μM	Made small to have little impact relative to other buffers
Myosin	γ_{cross}	17 $(\mu\mathrm{M})^{-3}$ s^{-1}	Yang et al. [71]
	K_1	$\gamma_{\mathrm{cross}}[\mathrm{Ca}^{2+}]^3_{\mathrm{cyt}}$	
	K_2	0.5 s^{-1}	
	K_3	0.4 s^{-1}	
	K_4	0.1 s^{-1}	
	K_5	0.5 s^{-1}	
	K_6	$\gamma_{\mathrm{cross}}[\mathrm{Ca}^{2+}]^3_{\mathrm{cyt}}$	
	K_7	0.1 s^{-1}	
$\mathrm{IP}_3 + \mathrm{PIP}_2$	η_{IP_3}	11.725 $(\mu\mathrm{M}\cdot\mathrm{s})^{-1}$	Lemon et al. [47]
	$k_{\mathrm{deg,IP}_3}$	1.25 s^{-1}	
	k_{c}	0.4 μM	
	$[\mathrm{PIP}_2]_{\mathrm{rr}}$	0.1 s^{-1}	
	$[\mathrm{PIP}_2]_{\mathrm{tot}}$	118.61 μM	Johny et al. [39]

Table 1: Cytosol-specific model parameters.

with fixed parameters in Table 1.

The tension generated by the smooth muscle cell is a linear function

$$F_r \propto (\mathrm{AMp} + \mathrm{AM})$$

of the total associated actin-associated myosin. Since three calcium ions are effectively buffered when myosin is in either the Mp or AMp states, myosin binding induces a change in cytosolic free calcium given by the reaction flux

$$J_{\mathrm{cyt}\to\mathrm{cyt}} = -[\mathrm{Myo}]\frac{\mathrm{d}}{\mathrm{d}t}(\mathrm{Mp} + \mathrm{AMp})\,. \tag{6}$$

The disassociation of myosin from actin is energy dependent. For the sake of simplicity, we assume that ATP production meets the needs of this system.

The remaining contributors to cytosolic calcium changes lie in the specific mechanisms through which the cytosol interacts with the other compartments. Inositol trisphosphate, (IP_3), is an important modulator of these interactions. We model the dynamics of of IP_3 using the model of Lemon et al. [47], where

$$\frac{\mathrm{d}[\mathrm{IP}_3]}{\mathrm{d}t} = r_h[\mathrm{PIP}_2] - k_{\mathrm{deg,IP}_3}[\mathrm{IP}_3], \tag{7}$$

which is coupled to the dynamics for phosphatidylinositol (4,5)-bisphosphate (PIP_2)

$$\frac{\mathrm{d}[\mathrm{PIP}_2]}{\mathrm{d}t} = -(r_h + [\mathrm{PIP}_2]_{\mathrm{rr}})\cdot[\mathrm{PIP}_2] + [\mathrm{PIP}_2]_{\mathrm{rr}}\cdot([\mathrm{PIP}_2]_{\mathrm{tot}} - [\mathrm{IP}_3]). \tag{8}$$

Note that we only model IP_3 and PIP_2 in the cytosolic compartment - for this reason we drop the cytosolic subscript. Both Eqs. 7 and 8 are sensitive to cytosolic calcium concentration due to the relationship

$$r_h = \eta_{\mathrm{IP}_3}\frac{[\mathrm{Ca}^{2+}]_{\mathrm{cyt}}}{k_c + [\mathrm{Ca}^{2+}]_{\mathrm{cyt}}}[\mathrm{G}], \tag{9}$$

where the concentration of G-protein $[\mathrm{G}] = 3.314\times10^{-5}$ μM is assumed to be fixed.

	Parameter	Value	Notes
	ν_{mcu}	4.4×10^{-6} μM/s	Wacquier et al. [65] adjusted based on Williams et al. [69] Figure 2D
	ν_{nclx}	0.13 μM/s	
	k_{c}	0.4 μM	Wacquier et al. [65]
	$\Delta\Psi_m$	140 mV	

Table 2: Mitochondria model parameters.

2.2 Mitochondria

In the mitochondria, we assume that there is an excess of calcium and that calcium-phosphate clusters have formed. Additionally, we assume that this process has come to equilibrium so that calcium and phosphate are balanced at their saturation concentrations. By conservation, the mitochondrial calcium concentration obeys

$$\frac{\mathrm{d}[\mathrm{Ca}^{2+}]_{\text{mit}}}{\mathrm{d}t} = J_{\text{mit}\to\text{mit}} - J_{\text{mit}\to\text{cyt}}, \tag{10}$$

where $J_{\text{mit}\to\text{mit}}$ accounts for the exchange of calcium between the free solution and clusters. We make the assumption that this exchange is rapid, relative to exchange with the cytosol. Hence, making the leading order quasi-steady state assumption implies that $J_{\text{mit}\to\text{mit}} = 0 + \mathcal{O}(\varepsilon)$ as the system evolves, where $\varepsilon \ll 1$ is a small parameter. $J_{\text{mit}\to\text{mit}}$ is zero when $[\mathrm{Ca}^{2+}]_{\text{mit}}$ is exactly at saturation; these assumptions imply that $[\mathrm{Ca}^{2+}]_{\text{mit}}$ is a constant so long as clusters are not depleted and the composition of the solution does not change drastically. For these conditions to hold, we make the additional assumptions that the pH and concentration of phosphate are held nearly constant by other processes which we do not explicitly model.

Excess mitochondrial calcium is the driver for perturbations in calcium dynamics in our model, where we include three explicit mechanisms for calcium exchange between mitochondria and the cytosol. Although the free ionic calcium concentration within the mitochondria is fixed, due to supersaturation, the net amount of calcium present within the mitochondria varies as a result of exchange with the cytosol. In normal physiology, mitochondria are calcium buffers of last resort, taking in calcium through a combination of the mitochondrial calcium uniporter (MCU) and the mitochondrial sodium calcium exchanger (NCLX). Parameter values particular to the mitochondria are in Table. 2.

We assume that the flux through the uniporter is unidirectional, with rate given by

$$J_{\text{mcu}} = -\nu_{\text{mcu}} \frac{\dfrac{[\mathrm{Ca}^{2+}]_{\text{cyt}}}{K_{\text{mcu},1}} \left(1 + \dfrac{[\mathrm{Ca}^{2+}]_{\text{cyt}}}{K_{\text{mcu},1}}\right)^3}{\left(1 + \dfrac{[\mathrm{Ca}^{2+}]_{\text{cyt}}}{K_{\text{mcu},1}}\right)^4 + \dfrac{L_{\text{mcu}}}{\left(1 + \dfrac{[\mathrm{Ca}^{2+}]_{\text{cyt}}}{K_{\text{mcu},2}}\right)}}. \tag{11}$$

The NCLX is a bidirectional channel. We model its calcium flux through the expression

$$J_{\text{nclx}} = \nu_{\text{nclx}} \left(\frac{[\mathrm{Ca}^{2+}]_{\text{mit}}}{[\mathrm{Ca}^{2+}]_{\text{cyt}}}\right) e^{p_2 \Delta\Psi_m}, \tag{12}$$

where the mitochondrial membrane potential $\Delta\Psi_m$ is considered fixed. Finally, we model an Ohmic leak through non-specific mechanisms as

$$J_{\text{mit,leak}} = -\nu_{\text{mit,leak}} \left(\Delta\Psi_m - E_{\text{Ca,mit}}\right), \tag{13}$$

where the mitochondrial calcium Nernst potential is

$$E_{\text{Ca,mit}} = \frac{RT}{2F} \log\left(\frac{[\mathrm{Ca}^{2+}]_{\text{mit}}}{[\mathrm{Ca}^{2+}]_{\text{cyt}}}\right). \tag{14}$$

The conductance of the leak current is set so that the mitochondrial flux is zero when $[\mathrm{Ca}^{2+}]_{\text{mit}} = [\mathrm{Ca}^{2+}]_{\text{cyt}} = 0.1$ μM. We express the net flux between the mitochondrial compartment and cytosol as a sum over the three contributors,

$$J_{\text{mit}\to\text{cyt}} = J_{\text{mcu}} + J_{\text{nclx}} + J_{\text{mit,leak}}. \tag{15}$$

2.3 Endoplasmic reticulum

Via exchange with the cytosol, the ER calcium concentration follows

$$\frac{\mathrm{d}[\mathrm{Ca}^{2+}]_{\mathrm{er}}}{\mathrm{d}t} = -\frac{r_{\mathrm{er}}^{\mathrm{cyt}}}{b_{\mathrm{er}}} J_{\mathrm{er}\to\mathrm{cyt}} \tag{16}$$

with dynamic buffering given

$$b_{\mathrm{er}} = 1 + \frac{K_{\mathrm{CalrC}}[\mathrm{CalrC}]_{\mathrm{er}}}{\left(K_{\mathrm{CalrC}} + [\mathrm{Ca}^{2+}]_{\mathrm{er}}\right)^2} + \frac{K_{\mathrm{CalrP}}[\mathrm{CalrP}]_{\mathrm{er}}}{\left(K_{\mathrm{CalrP}} + [\mathrm{Ca}^{2+}]_{\mathrm{er}}\right)^2}. \tag{17}$$

where all quantities are fixed and listed in Table 3.

Within the ER, we model the interplay between calcium intake through the ubiquitous sarco/endo-plasmic reticulum (SERCA) buffering protein and calcium-induced-calcium-release (CICR) through the calcium-triggered ryanodine receptors (RyR) and IP_3-sensitive receptors (IP_3Rs). Hence, we write

$$J_{\mathrm{er}\to\mathrm{cyt}} = J_{\mathrm{serca}} + J_{\mathrm{ryr}} + J_{\mathrm{ipr}}. \tag{18}$$

2.3.1 Sarco/endoplasmic reticulum Ca^{2+}-ATPase

The ER, through the SERCA pump protein, is the primary cellular calcium buffer under physiological conditions. SERCA hydrolyzes ATP to pump calcium against its gradient into the ER, where free ionic calcium is two orders of magnitude more concentrated than in the cytosol. We model the action of SERCA using the bufferless approximation of Higgins et al. [36],

$$J_{\mathrm{serca}} = \frac{2\left(-K_1^2K_3^2k_{-2}k_{-4}[\mathrm{Ca}^{2+}]_{\mathrm{er}}^2 + k_2k_4[\mathrm{Ca}^{2+}]_{\mathrm{cyt}}^2\right)[\mathrm{SERCA}]}{[\mathrm{Ca}^{2+}]_{\mathrm{er}}^2[\mathrm{Ca}^{2+}]_{\mathrm{cyt}}^2K_3^2\left(k_2+k_{-2}\right) + [\mathrm{Ca}^{2+}]_{\mathrm{cyt}}^2\left(k_4+k_2\right) + [\mathrm{Ca}^{2+}]_{\mathrm{er}}^2K_1^2K_3^2\left(k_{-2}+k_{-4}\right) + K_1^2\left(k_4+k_{-4}\right)}, \tag{19}$$

where the model parameters are given in Table 3.

2.3.2 IP_3 receptors

For determining flux through IP_3R, we used the four-state channel model of Swaminathan et al. [60], The whole-cell IP_3R flux is given by

$$J_{\mathrm{ipr}} = \nu_{\mathrm{ipr}}\left(X_{10}^4 + 4X_{10}^3(1-X_{10})\right)\left([\mathrm{Ca}^{2+}]_{\mathrm{er}} - [\mathrm{Ca}^{2+}]_{\mathrm{cyt}}\right), \tag{20}$$

where X_{10} is modeled by the dynamical system

$$\begin{pmatrix}\dot{X}_{00}\\ \dot{X}_{01}\\ \dot{X}_{10}\end{pmatrix} = \begin{pmatrix}0\\ b_5\\ b_2\end{pmatrix} + \begin{bmatrix} -\dfrac{(a_4k_1+a_5+a_2)[\mathrm{Ca}^{2+}]_{\mathrm{cyt}}}{1+k_1} & \dfrac{b_4k_3+b_2}{1+k_3} & b_5 \\ \dfrac{(a_4k_1+a_2)[\mathrm{Ca}^{2+}]_{\mathrm{cyt}}}{1+k_1} - b_5 & -\dfrac{b_4k_3+b_2+a_5[\mathrm{Ca}^{2+}]_{\mathrm{cyt}}}{1+k_3} - b_5 & -b_5 \\ \dfrac{a_5[\mathrm{Ca}^{2+}]_{\mathrm{cyt}}}{1+k_1} - b_2 & -b_2 & -a_2[\mathrm{Ca}^{2+}]_{\mathrm{cyt}} - b_5 - b_2 \end{bmatrix}\begin{pmatrix}X_{00}\\ X_{01}\\ X_{10}\end{pmatrix} \tag{21}$$

The fourth state has been eliminated using the conservation condition.

	Parameter	Value	Notes
Buffer	K_{CalC}	2×10^3 μM	Adjusted down from Means et al. [49] to yield $[Ca^{2+}]_{er,tot} \approx 2$ mM at rest
	$[\mathrm{CalC}]_{\mathrm{er}}$	7.2×10^3 μM	
	K_{CalP}	10 μM	
	$[\mathrm{CalP}]_{\mathrm{er}}$	7.2×10^2 μM	
SERCA	K_1	$\sqrt{0.7}$ μM	Higgins et al. [36]
	K_3	$\sqrt{1.111111 \times 10^{-5}}$ μM	
	k_2	$0.6 \times \xi$ s^{-1}	
	k_{-2}	$0.97 \times \xi$ s^{-1}	
	k_4	$0.4 \times \xi$ s^{-1}	
	k_{-4}	$1.2 \times 10^{-3} \times \xi$ s^{-1}	
	[SERCA]	182 μM	Fitted to balance ER fluxes at steady state
	ξ	10	
IP_3R	ν_{ipr}	1000 s^{-1}	Reduced from [39] to allow for balance using physiologically plausible SERCA concentration
	a_1	167.6 $(\mu M)^{-1}$ s^{-1}	Swaminathan et al. [60]
	a_2	3.81 $(\mu M)^{-1}$ s^{-1}	
	a_3	413.4 $(\mu M)^{-1}$ s^{-1}	
	a_4	0.3101 $(\mu M)^{-1}$ s^{-1}	
	a_5	53.9 $(\mu M)^{-1}$ s^{-1}	
	b_1	228 s^{-1}	
	b_2	0.409 s^{-1}	
	b_3	188.5 s^{-1}	
	b_4	0.096 s^{-1}	
	b_5	4.52 s^{-1}	
RyR	ν_{ryr}	0.2 s^{-1}	Decreased from Johny et al. [39] to decrease oscillation magnitudes
	K_{r1}	2.5 $(\mu M)^{-2}$ s^{-1}	Yang et al. [71]
	K_{r2}	1.5 $(\mu M)^{-1}$ s^{-1}	
	K_{-r1}	7.6 s^{-1}	
	K_{-r2}	84 s^{-1}	

Table 3: ER model parameters

2.3.3 Ryanodine receptors

For the RyR, we used a similar four-state system governed by the dynamics

$$\begin{pmatrix} \dot{R}_{10} \\ \dot{R}_{11} \\ \dot{R}_{01} \end{pmatrix} = \begin{pmatrix} K_{r1}[\mathrm{Ca}^{2+}]_{\mathrm{cyt}}^2 \\ 0 \\ K_{r2}[\mathrm{Ca}^{2+}]_{\mathrm{cyt}} \end{pmatrix} + \begin{bmatrix} -(K_{-r1} + K_{r2}[\mathrm{Ca}^{2+}]_{\mathrm{cyt}}) - K_{r1}[\mathrm{Ca}^{2+}]_{\mathrm{cyt}}^2 & K_{-r2} - K_{r1}[\mathrm{Ca}^{2+}]_{\mathrm{cyt}}^2 & -K_{r1}[\mathrm{Ca}^{2+}]_{\mathrm{cyt}}^2 \\ K_{r2}[\mathrm{Ca}^{2+}]_{\mathrm{cyt}} & -K_{-r1} - K_{-r2} & K_{r1}[\mathrm{Ca}^{2+}]_{\mathrm{cyt}}^2 \\ -K_{r2}[\mathrm{Ca}^{2+}]_{\mathrm{cyt}} & K_{-r1} - K_{r2}[\mathrm{Ca}^{2+}]_{\mathrm{cyt}} & K_{-r2} - K_{r1}[\mathrm{Ca}^{2+}]_{\mathrm{cyt}}^2 - K_{r2}[\mathrm{Ca}^{2+}]_{\mathrm{cyt}} \end{bmatrix} \times \begin{pmatrix} R_{10} \\ R_{11} \\ R_{01} \end{pmatrix}, \tag{22}$$

and

$$J_{\mathrm{ryr}} = \nu_{\mathrm{ryr}} R_{10}^2 \left([\mathrm{Ca}^{2+}]_{\mathrm{er}} - [\mathrm{Ca}^{2+}]_{\mathrm{cyt}} \right). \tag{23}$$

	Parameter	Value	Notes
	ϕ_{ecs}	-54 mV	Taken from Johny et al. [39]
	V_{cyt}	0.7 pL	
	η_{ecs}	0.35	
	$[\text{Na}^+]_{\text{ecs}}$	140 mM	
	$[\text{Na}^+]_{\text{cyt}}$	8 mM	
	d_{ncx}	$(0.01\ \mu\text{M})^{-4}$	Demir et al. [19]
	k_{ncx1}	$0.125\ \mu$M	
	Q_{pmca}	$0.04\ \mu\text{M s}^{-1}$	Adjusted from Demir et al. [19] and Johny et al. [39] to reproduce constriction from Chang et al. [13] Fig 4A, while balancing fluxes at steady state
	k_{ncx2}	$0.5\ \mu$A	
	$g_{\text{leak,ecs}}$	$3.0 \times 10^{-5}\ \mu\text{M}\ (\text{mV} \cdot s)^{-1}$	
	k_{pmca}	$0.15\ \mu$M	
	Q_{vocc}	$0.10\ \ \mu\text{M}\ (\text{mV} \cdot s)^{-1}$	
	F	$96487\ \text{C} \cdot \text{mol}^{-1}$	

Table 4: Plasma-membrane and extracellular specific model parameters

2.4 Plasma membrane

The interactions between the cytosol of the smooth muscle cell and the extracellular space that we consider are the calcium-dependent ones of Johny et al. [39], though the sodium-calcium exchanger (NCX) is taken from Demir et al. [19]. The NCX follows

$$J_{\text{ecs,ncx}} = \frac{k_{\text{ncx2}}}{2FV_{\text{cyt}}} \frac{([\text{Na}^+]_{\text{cyt}}^3[\text{Ca}^{2+}]_{\text{ecs}}\phi_F - [\text{Na}^+]_{\text{ecs}}^3[\text{Ca}^{2+}]_{\text{cyt}}\phi_R)}{(1 + d_{\text{ncx}}([\text{Ca}^{2+}]_{\text{cyt}}[\text{Na}^+]_{\text{ecs}}^3 + [\text{Ca}^{2+}]_{\text{ecs}}[\text{Na}^+]_{\text{cyt}}^3))} \frac{1}{1 + \left(\frac{k_{\text{ncx1}}}{[\text{Ca}^{2+}]_{\text{cyt}}}\right)^2}. \tag{24}$$

The Voltage-gated calcium channel (VOCC) follows

$$J_{\text{vocc}} = -Q_{\text{vocc}}\bar{d}_l\bar{f}_l(\phi_{\text{ecs}} - E_{\text{Ca,ecs}}), \tag{25}$$

where

$$E_{\text{Ca,ecs}} = \frac{RT}{2F}\log\left(\frac{[\text{Ca}^{2+}]_{\text{ecs}}}{[\text{Ca}^{2+}]_{\text{cyt}}}\right), \tag{26}$$

$$\phi_F = \exp\left(\eta_{\text{ncx}}\phi_{\text{ecs}}\frac{F}{RT}\right), \quad \phi_R = \exp\left((\eta_{\text{ncx}} - 1)\phi_{\text{ecs}}\frac{F}{RT}\right), \tag{27}$$

$$\bar{d}_l = \frac{1}{\left(1 + \exp\left(-\frac{\phi_{\text{ecs}}}{8.3\ \text{mV}}\right)\right)}, \quad \text{and} \quad \bar{f}_l = \frac{1}{\left(1 + \exp\left(\frac{(\phi_{\text{ecs}} + 42\ \text{mV})}{9.1\ \text{mV}}\right)\right)}. \tag{28}$$

The non-specific leak and (Plasma membrane Ca2+ ATPase) PMCA follow

$$J_{\text{ecs,leak}} = -g_{\text{leak,ecs}}(\phi_{\text{ecs}} - E_{\text{Ca,ecs}}) \tag{29}$$

$$J_{\text{pmca}} = -Q_{\text{pmca}}\frac{[\text{Ca}^{2+}]_{\text{cyt}}}{[\text{Ca}^{2+}]_{\text{cyt}} + k_{\text{pmca}}}. \tag{30}$$

Overall,

$$J_{\text{ecs}\to\text{cyt}} = J_{\text{ecs,leak}} + J_{\text{pmca}} + J_{\text{ecs,ncx}} + J_{\text{vocc}}. \tag{31}$$

2.5 Tracking calcium clearance

We assume that the extracellular space is a bulk bath, thereby assuming that $[\text{Ca}^{2+}]_{\text{ecs}} = 1.3$ mM. Yet, while the ECS is assumed to have a constant concentration, we still track the net calcium flow from the cytosol to the ECS, through mass balance, using the differential equation

$$\frac{\text{d}[\text{Ca}^{2+}]_{\text{sink}}}{\text{d}t} = -J_{\text{ecs}\to\text{cyt}}. \tag{32}$$

Similarly, we assume that the calcium concentration is fixed at an elevated state determined by equilibrium solubility of calcium and phosphate, under the assumption that both species are in excess and that the pH is stable. However, we track the net release of calcium from the mitochondria through the differential equation

$$\frac{\mathrm{d}[\mathrm{Ca}^{2+}]_{\mathrm{source}}}{\mathrm{d}t} = J_{\mathrm{mit}\to\mathrm{cyt}}. \tag{33}$$

The net rate of calcium release from the cell is the primary quantity of interest in our model, as it provides a picture of the overall timescale of perturbed calcium dynamics.

The leakage of calcium from mitochondria is what drives the dynamics in our model. Due to stoichiometric considerations, leakage corresponds to calcium dissolution which also affects the pH within the mitochondria. Due to this fact, the leakage of calcium from the mitochondria also implies a driving source of ATP production.

2.6 Contribution of dissolution to ATP production

Aerobic ATP production is driven by energy from the proton gradient between the mitochondrial matrix and the mitochondrial inner membrane. In aerobic conditions, this gradient is maintained by proton pumps in the electron transport chain [33]. Protons within the inner mitochondrial membrane are in passive exchange with the bulk cytosol. The pumps move protons from the matrix into the inner membrane. They are extremely efficient; on average only a small number of protons are present within each mitochondrial matrix, maintaining a stable alkaline environment of pH ≈ 7.8 [55]. Hence, the main determinant of the gradient is the absence or presence of protons in the matrix.

The mitochondrial F_0F_1-ATP synthase harnesses the passive flux of protons through its inner pore, in order to produce ATP from ADP and free inorganic phosphate. Being reversible, this mechanism depends crucially on maintenance of the gradient, typically by oxidative phosphorylation. Any process that removes protons from the mitochondrial matrix helps to sustain ATP production, where an estimated three protons contributes to the production of an ATP molecule [1].

Liberation of calcium also results in liberation of free inorganic phosphate and hydroxide ions, both of which associate with protons. Hence, calcium phosphate dissolution can have an energetically protective effect by sustaining aerobic respiration in anaerobic settings. We quantify the resulting rate of ATP production through this mechanism by noting that the production rate is proportional to $J_{\mathrm{mit}\to\mathrm{cyt}}$, under the assumption of quasi-steady equilibrium in the interplay between dissolution and aggregation.

2.7 Steady-state parameterization

Our mathematical model has several free parameters. To constrain the dimensionality of these parameters, we enforce the steady-state conditions presented in Table 5.

	State	Value	Notes
	$[\mathrm{Ca}^{2+}]_{\mathrm{cyt}}$	0.1 μM	Hill-Eubanks et al. [37]
	$[\mathrm{Ca}^{2+}]_{\mathrm{ecs}}$	1300 μM	Hansen and Zeuthen [32]
	$[\mathrm{Ca}^{2+}]_{\mathrm{mit}}$	0.1 μM	Wacquier et al. [65]
	$[\mathrm{Ca}^{2+}]_{\mathrm{er}}$	500 μM	Free calcium estimate within the range given by Demaurex and Frieden [18]

Table 5: **Steady state free ionic calcium concentrations** enforced in all of our model simulations.

3 Results

We implemented our model in Julia 1.1 using `DifferentialEquations.jl` [57], with source code available at `github:joshchang/postcsd_calcium`. We used the default stiff ODE solver (called with `alg_hints=[:stiff]`), which was sufficiently stable at automatic step sizes to yield solutions at the default relative tolerance of 10^{-6}. In each of our simulations, all of the state variables in our model are initialized to satisfy steady-state concentrations for free calcium. We present results relative to a baseline parameter regime with behavior matching the vascular dynamics seen in [13]. We ascertained the frequency of any oscillations using `DSP.jl`.

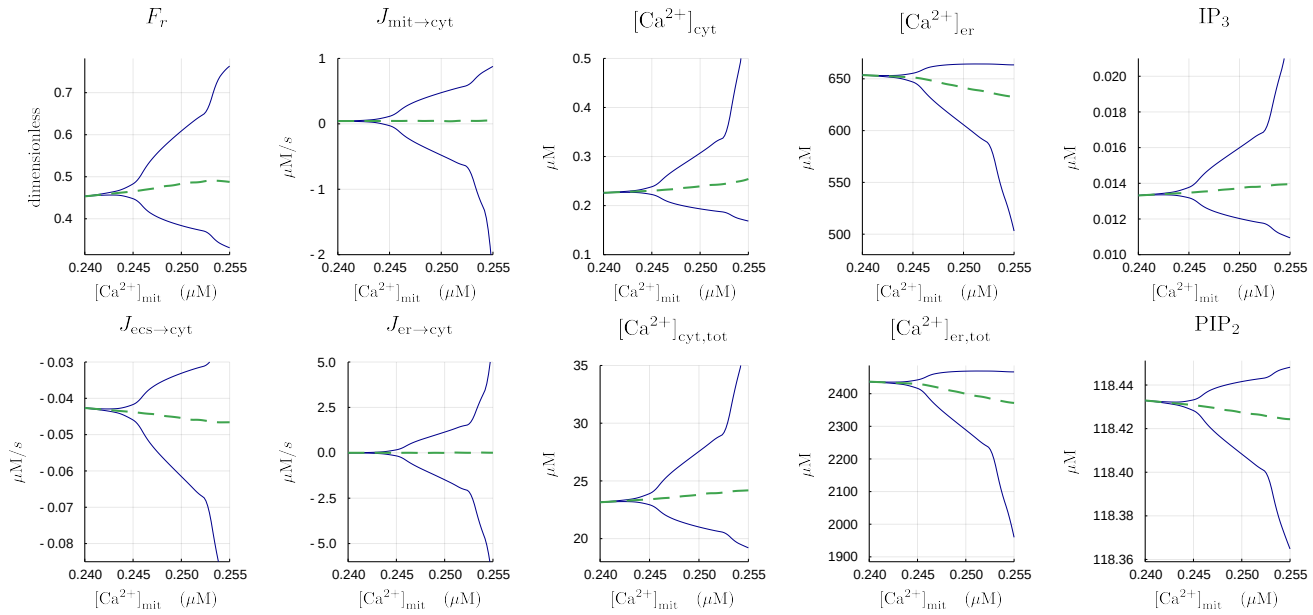

Figure 2: **Hopf bifurcation diagrams** as a function of $[\mathrm{Ca}^{2+}]_{\mathrm{mit}}$. A supercritical Hopf bifurcation initiates at around $[\mathrm{Ca}^{2+}]_{\mathrm{mit}} \approx 0.245$ μM. The period-averaged value for each variable is shown in dashed-green. F_r is proportional to the constrictive force generated by the smooth muscle cell.

3.1 Effect of elevations in $[\mathrm{Ca}^{2+}]_{\mathrm{mit}}$

We first fixed the model parameters to the reference values in Tables 1, 4, and 5; the only free parameter was the free ionic calcium concentration within the mitochondria. In these simulations the stabilizing leak fluxes are calibrated in order to maintain the original unperturbed steady state.

Fig. 2 shows the bifurcation from steady state to oscillatory cytosolic calcium dynamics above a critical threshold for $[\mathrm{Ca}^{2+}]_{\mathrm{mit}} \approx 0.245$ μM. The magnitude of these oscillations increases with the mitochondrial calcium concentration. The same bifurcation is present in the other model variables, for instance, the fraction of myosin light chain in the force-generating state (F_r). Although the net movement of calcium is from the mitochondria, to the cytosol, to the extracellular space, the direction of this flow oscillates as well.

Fig. 3 presents time courses of $[\mathrm{Ca}^{2+}]_{\mathrm{mit}} = 0.25$ μM. A transient period of approximately three minutes characterizes these simulations, where calcium from the mitochondria loads into the cytosol, primarily into the endoplasmic reticulum as shown in both the free and total calcium concentrations. The loading is primarily through action of SERCA, and is counteracted by calcium induced calcium release (CICR) through the IP_3R and ryanodine receptor channels.

The dynamics in this set of simulations are consistent with the observed vasoactivity of Figure 4A in Chang et al. [13]. Fig. 4 represents the macroscale physiological implications of the cellular calcium dynamics from Fig. 3. In half an hour, approximately 80 μM of free calcium is expelled from the cell ($[\mathrm{Ca}^{2+}]_{\mathrm{sink}}$), where the concentration is relative to the cytosolic volume. More calcium leaves the mitochondria ($[\mathrm{Ca}^{2+}]_{\mathrm{source}}$), with the difference accounted for by the combination of cytosolic and cellular buffers. Together, these two variables determine the timescale over which excess calcium in the mitochondrial matrix is depleted. Concomitant with the calcium dynamics, oscillatory vascular dynamics within a range of constrictions is predicted.

We study the parametric determinants of calcium dynamics in our model by looking at the impact of changing the flux through a hundred-fold rescaling via

$$J_{(\cdot)\to\mathrm{cyt}} \to \alpha_{(\cdot)} J_{(\cdot)\to\mathrm{cyt}}. \tag{34}$$

Note that these transformations preserve steady state in our model because the model is calibrated to zero flux at the prescribed steady state described in the aforementioned tables. Fig. 5 shows how rescalings of the three fluxes, for $\alpha_{(\cdot)} \in [0.1, 10]$, affect the presence of stable oscillations in cytosolic calcium concentration. From these simulations, it is clear that the endoplasmic reticulum is crucial for the development of oscillations. There were no oscillations observed for $\log_{10} \alpha_{\mathrm{er}} \lessapprox -0.5$.

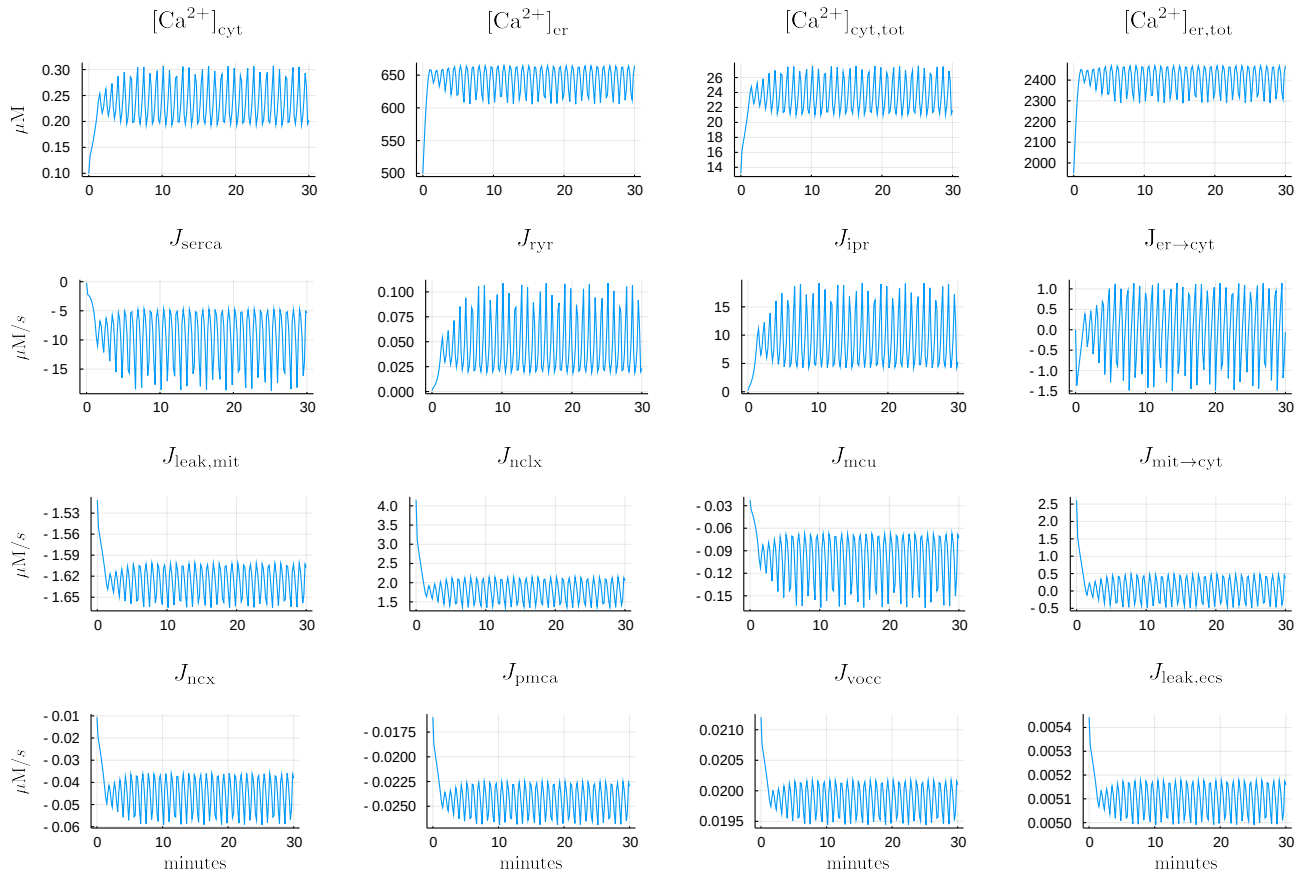

Figure 3: **Model time courses** for $[Ca^{2+}]_{mit} = 0.25\ \mu M$. Positive fluxes correspond to flow into the cytosol. We distinguish between free and total calcium in each of the ER and cytosol. Mitochondrial calcium assumed to be in quasi-steady equilibrium with respect to dissolution and aggregation.

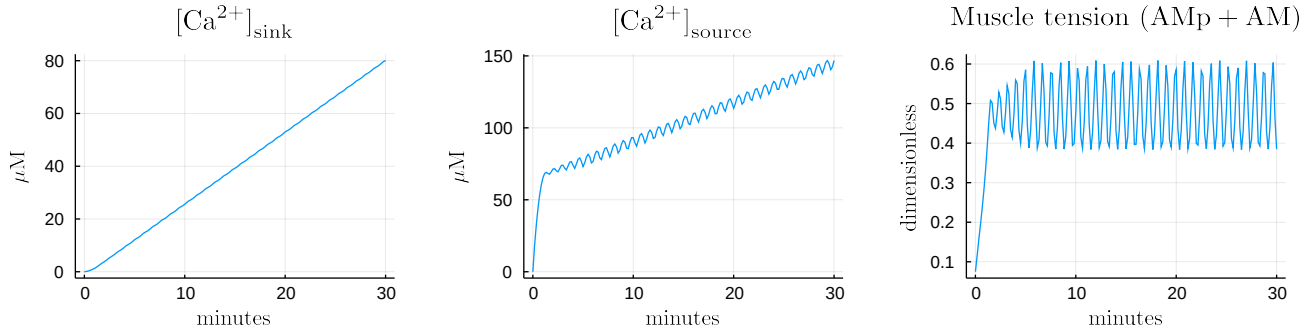

Figure 4: **Cumulative calcium movement and vascular activity** as a consequence of elevated mitochondrial calcium ($[Ca^{2+}]_{mit} = 0.25\ \mu M$). Sink refers to the cumulative calcium exiting the cell and entering the ECS. Source refers to the cumulative calcium exiting the mitochondrial matrix. All concentrations relative to the cytoplasmic volume which is assumed to be 0.7 pL.

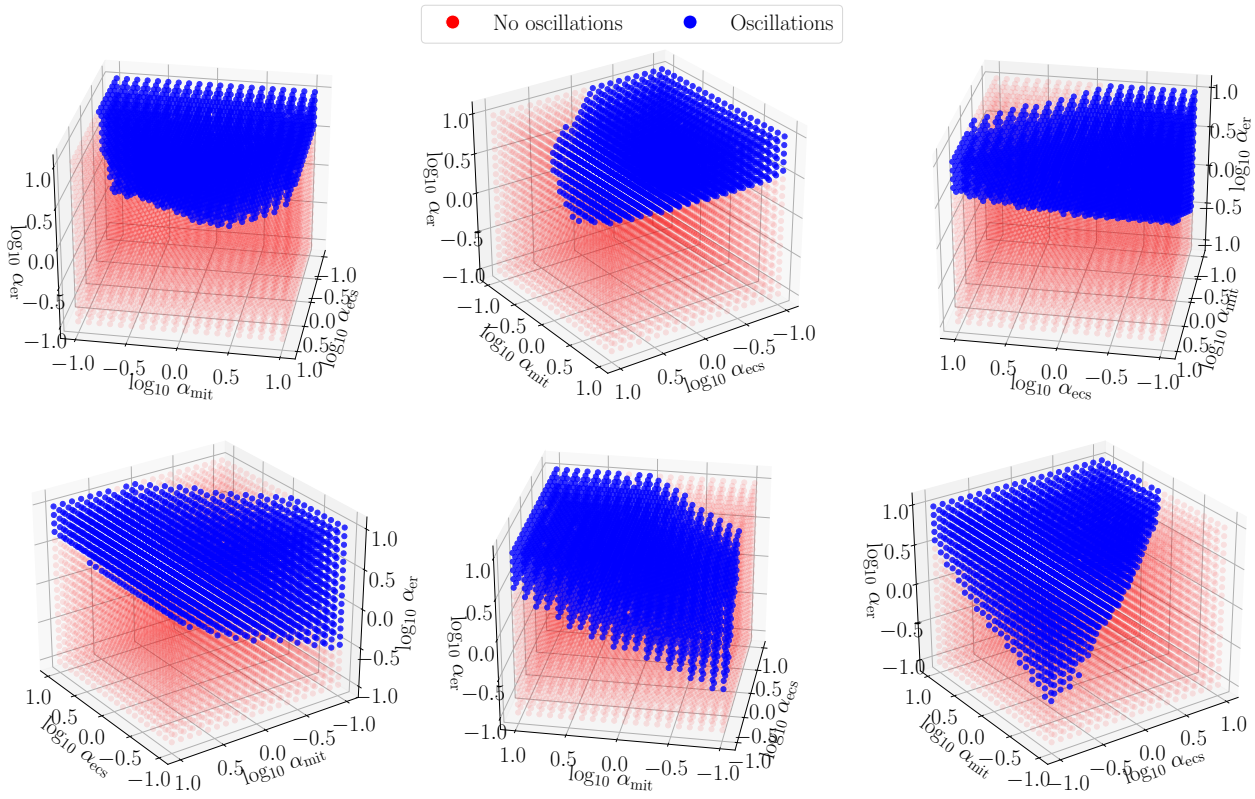

Figure 5: **Presence of oscillations** as a function of flux rescalings defined in Eq. 34.

3.2 Determinants of timescale

As shown in Fig. 2, elevations in $[Ca^{2+}]_{mit}$ drive changes in calcium dynamics. The persistence of these perturbations depends on the timescale over which calcium remains elevated in the mitochondria, which is controlled by the rate of calcium extrusion. Eqs. 32 and 33 describe the cumulative extrusion of calcium from the mitochondria and the cell respectively, as shown in Fig. 4.

In Fig. 6, for $\log_{10}\alpha_{(\cdot)} \in [-1, 1]$, we present the effect of the flux rescalings on the overall rate of calcium extrusion from the cell, conditional on the presence or absence of oscillations. It is evident that the presence of oscillations does not impact the rate of efflux – as shown in the first panel, $J_{ecs\to cyt}$ is largely independent of α_{er} as long as the two other rescalings are taken into account. The magnitude of the flux also increases sub-linearly with respect to increase of the mitochondrial fluxes though nearly linearly with respect to plasma membrane rescaling. The kinetics of the plasma membrane mechanics are the main determinant of net extrusion rate.

At rest, the extracellular space comprises approximately 20% of the cerebral tissue volume [51, 61], with a resting ionic calcium concentration of approximately 1.3 mM. At the peak of CSD, the extracellular calcium concentration drops to under 0.1 mM while its volume fraction drops by half. To understand the timescale implied in the simulations of Fig. 3 and Fig. 6, suppose that there is only one cell type within the tissue, that comprises the remaining 80% of the volume, and absorbs all of the calcium from the ECS during CSD. If we assume conservatively that, due to the volume ratios, calcium dilutes by a factor of four in the cytosol, an effective concentration of over 300 μM enters into these cells. However, the cells would not experience elevations of free calcium near the level in the cytosol since the calcium would be buffered. If the mitochondria absorb approximately a third of this excess calcium, then the simulation of Fig. 3 predicts a timescale of over 30 minutes to expel the absorbed calcium.

In all of these simulations, the direction of the net calcium flux at 30 minutes is out of the cell. However, as shown in Fig. 7, there are a minority of simulations whose parameter sets yielded a net inward mitochondrial flux at 30 minutes. These simulations were associated with large mitochondria rescalings concomitant with large ER rescalings, demonstrating a net emptying of the ER stores into the mitochondria.

In the majority of simulations, there is a net emptying of mitochondria. This emptying proceeded at a slow rate in the absence of oscillations. In the presence of oscillations, larger net fluxes can be observed, with the caveat that the oscillations can result in periods where the fluxes reverse, as present in the simulation presented in Fig. 3. Relative

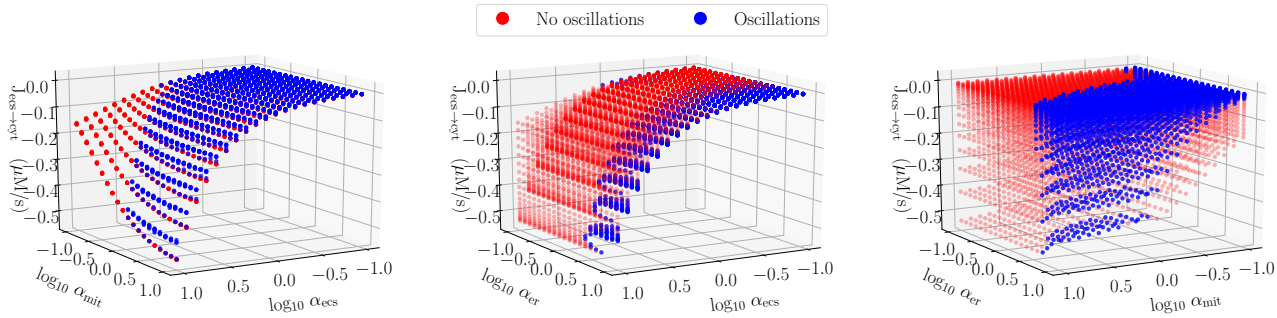

Figure 6: **The net period-averaged calcium flux between the extracellular space and cytosol** as the channel and pump rates are rescaled according to Eq. 34. Left to right: flux as a function of mitochondrial and plasma membrane rescaling, as a function of ER and plasma membrane rescaling, and as a function of ER and mitochondrial rescaling. Blue denotes the presence of stable oscillations.

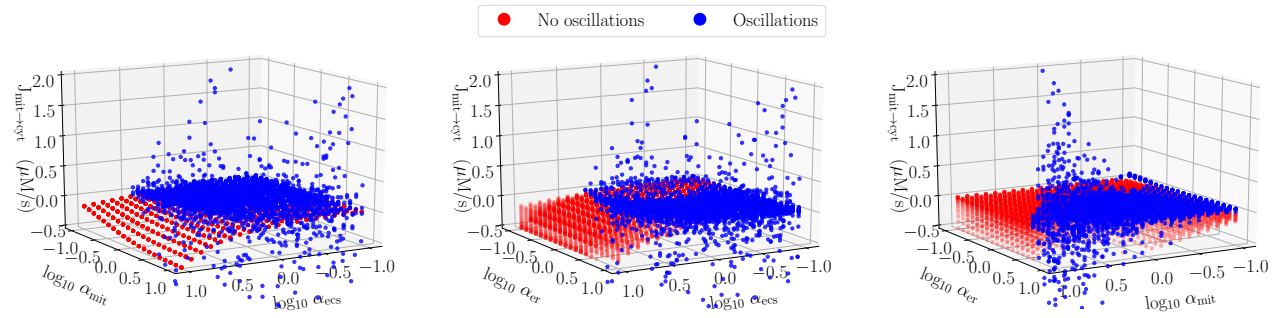

Figure 7: **Period-averaged flux from mitochondria to cytosol** with presence of oscillations indicated. Approximately 8% of simulations had net flux into the mitochondria at the end of 30 minutes. The majority had flux out of the mitochondria, with oscillatory simulations exhibiting larger average fluxes.

to the mitochondrial matrix, outward fluxes imply calcium dissolution, proton consumption, and ATP production. Inward fluxes result in the opposite.

4 Discussion

We have presented a model of calcium dynamics within smooth muscle vascular cells incorporating relevant endoplasmic reticulum, mitochondrial, and plasma-membrane dynamics that participate in responding to elevations in calcium concentration. Using this model, we demonstrated macroscopic vascular behavior consistent with the hour-long disruption in neurovascular coupling following cortical spreading depolarization.

On the macroscopic level, the phenotype we describe is the post-acute dynamics seen in the pial artery diameter measurement of Figure 4A of Chang et al. [13]. Following acute CSD, over the period of a few minutes, the diameter drops from a prior resting state to a persistent constrictive state lasting for over half an hour. While the vessel is constricted, small-amplitude oscillations are visible, consistent with the result of our model in Fig. 4. Note that the actual vascular radius is a function of the fluid pressures within the vasculature, the smooth muscle contractile force, and the tissue pressure. In our simulations, we only consider the contractile force.

Our chief modification to prior models has been the explicit handling of calcium buffering. Many prior studies assumed that a fixed proportion of calcium is buffered [6, 5, 66]. This assumption is an approximate form of the rapid buffer approximation that we use in this study. In particular, we distinguished between free and buffered calcium in the endoplasmic reticulum (ER). In doing so, we account for the finite capacity of the ER. The driving hypothesis of our paper is that solubility is essential for determining the recovery of calcium dynamics as affected by mitochondria after CSD. Solubility limits the rate of extrusion by reducing the active free ionic calcium concentration.

4.1 Assumptions, limitations, and alternative mechanisms

We account for solubility in the mitochondria by invoking a quasi-steady state assumption on the concentration of free calcium under the rapid equilibration of dissolution and aggregation of calcium phosphate species. The actual chemical pathways underlying these transformations are complex but we assume that they are rapid relative to the rate of exchange mechanisms present in the mitochondrial membrane.

In formulating our model, we inherited some assumptions of prior work [66, 30, 48, 39, 21, 40]. We relied on prior models for understanding the dynamical implications of elevated mitochondrial calcium and on measurements on mesenteric smooth rather than cerebral smooth muscle cells. In some cases, we have tuned the parameters to reflect this change, for instance, by tuning down the activity of RyR relative to IP_3R. A major challenge of quantitative study in this field is in parametric uncertainty, as many reported values in the literature are based on the fitting of under-determined systems. We have attempted to put ourselves in a physiologically reasonable parameter regime from which we did exploration. However, this work would benefit from quality cell-specific measurements of the enclosed mechanisms.

Prior models distilled the biological variability in vascular smooth muscle calcium dynamics into a few most-salient mechanisms which we replicate in our model. We made the simplifying assumptions of ignoring voltage-dependent calcium re-entry and the dependence on concentrations of other ions. Hence, our estimate of the recovery timescale may be low due to the fact that additional calcium entry or depletion of cofactors would increase the recovery time. Additionally, we neither modeled the energetic cascade behind ATP formation nor accounted for ATP depletion. This choice should also lead to an underestimate of recovery time. We believe our model represents a reasonable lower bound for vascular mitochondrial calcium recovery from CSD.

In our manuscript, we present a possible calcium-centric mitochondrial mechanism for vascular dysfunction. It should be noted, however, that there are other potential mechanisms of vascular origin that would cause long-lasting vasoconstriction. Since actin-myosin unbinding requires ATP, it could be the case that the smooth muscle cells are ATP starved. This starvation could be caused also through mitochondrial dysfunction resulting from mPTP opening.

4.2 Physiological implications

Using our model, we investigated the expulsion of excess calcium from the mitochondrial matrix conditional on the prior formation of calcium phosphate clusters. Prior experimental evidence [59] has shown that the clustering process can be rapid within mitochondria, with the saturation concentration being near the concentrations of $[Ca]_{mit}$ where we observe oscillations in our model.

Over half an hour, the simulation in Fig. 4 is able to clear approximately 80 μM of calcium from the cell into the extracellular space. While calcium oscillations are physiologically important, our model shows they are unimportant for determining the timescale of calcium elevation within the mitochondria. Rescaling the mitochondrial and plasma membrane fluxes, as shown in Fig. 6, modulates the recovery timescale whereas rescaling the ER flux has minimal effect, regardless of oscillations.

CSD is an universal phenomenon associated with many deleterious disorders. Its effects are both immediate and long-lasting. Much attention is paid to the role of neurons and glial cells in CSD. This manuscript is intended to shine a light on the vasculature itself as an active participant in its own dysregulation. Understanding the mechanisms behind the subacute CSD phase can aid in the development of treatments.

4.3 Possible protective effect

Calcium phosphate dissolution in the matrix directly consumes free protons, where approximately three protons removed from the matrix equates to a single ATP molecule. Hence, the rate of ATP production resulting from calcium phosphate dynamics is proportional to the flux shown in Fig. 7. When calcium flux out of the matrix is positive, the proton gradient is reinforced, supporting the production of ATP. Conversely, when the flux is negative, the proton gradient is compromised. If too many protons accumulate in the matrix, the F_0F_1-ATP synthase reverses and the enzyme consumes ATP rather than produces it.

On average, the flux out of the matrix is positive. Hence, not withstanding other negative effects on calcium dynamics, the dissolution process is partially protective in generating ATP through oxidative machinery, even in the absence of oxygen. However, as seen in Fig. 3, due to oscillations, there can be periods where the matrix calcium triggers calcium re-entry, working against the proton gradient.

Acknowledgments

Authors would like to thank Professors K.C. Brennan (University of Utah), R.S. Eisenberg (Rush Medical University) and Dr. J.M. Han (NIDDK). This research was supported in part by NSERC, the Fields Institute, and the Intramural Research Program of the NIH, NIDDK.

References

[1] Bruce Alberts, Alexander Johnson, Julian Lewis, Martin Raff, Keith Roberts, and Peter Walter. The Mitochondrion. *Molecular Biology of the Cell. 4th edition*, 2002. URL https://www.ncbi.nlm.nih.gov/books/NBK26894/.

[2] Cenk Ayata and Martin Lauritzen. Spreading Depression, Spreading Depolarizations, and the Cerebral Vasculature. *Physiological Reviews*, 95(3):953–993, July 2015. ISSN 0031-9333. doi: 10.1152/physrev.00027.2014. URL https://www.ncbi.nlm.nih.gov/pmc/articles/PMC4491545/.

[3] Trent A. Basarsky, Steven N. Duffy, R. David Andrew, and Brian A. MacVicar. Imaging Spreading Depression and Associated Intracellular Calcium Waves in Brain Slices. *The Journal of Neuroscience*, 18(18): 7189–7199, September 1998. ISSN 0270-6474, 1529-2401. doi: 10.1523/JNEUROSCI.18-18-07189.1998. URL http://www.jneurosci.org/lookup/doi/10.1523/JNEUROSCI.18-18-07189.1998.

[4] Heidi K. Baumgartner, Julia V. Gerasimenko, Christopher Thorne, Pawel Ferdek, Tullio Pozzan, Alexei V. Tepikin, Ole H. Petersen, Robert Sutton, Alastair J. M. Watson, and Oleg V. Gerasimenko. Calcium Elevation in Mitochondria Is the Main Ca2+ Requirement for Mitochondrial Permeability Transition Pore (mPTP) Opening. *Journal of Biological Chemistry*, 284(31):20796–20803, July 2009. ISSN 0021-9258, 1083-351X. doi: 10.1074/jbc.M109.025353. URL http://www.jbc.org/content/284/31/20796.

[5] Daniel A. Beard. A Biophysical Model of the Mitochondrial Respiratory System and Oxidative Phosphorylation. *PLOS Computational Biology*, 1(4):e36, September 2005. ISSN 1553-7358. doi: 10.1371/journal.pcbi.0010036. URL https://journals.plos.org/ploscompbiol/article?id=10.1371/journal.pcbi.0010036.

[6] Richard Bertram, Morten Gram Pedersen, Dan S. Luciani, and Arthur Sherman. A simplified model for mitochondrial ATP production. *Journal of Theoretical Biology*, 243 (4):575–586, December 2006. ISSN 0022-5193. doi: 10.1016/j.jtbi.2006.07.019. URL http://www.sciencedirect.com/science/article/pii/S0022519306003225.

[7] Jos A. M. Borghans, Rob J. de Boer, and Lee A. Segel. Extending the quasi-steady state approximation by changing variables. *Bulletin of Mathematical Biology*, 58(1):43–63, January 1996. ISSN 1522-9602. doi: 10.1007/BF02458281. URL https://doi.org/10.1007/BF02458281.

[8] James Bouley, David Y. Chung, Cenk Ayata, Robert H. Brown, and Nils Henninger. Cortical Spreading Depression Denotes Concussion Injury. *Journal of Neurotrauma*, 36(7):1008–1017, April 2019. ISSN 1557-9042. doi: 10.1089/neu.2018.5844.

[9] K. C. Brennan and Daniela Pietrobon. A Systems Neuroscience Approach to Migraine. *Neuron*, 97(5):1004–1021, March 2018. ISSN 0896-6273. doi: 10.1016/j.neuron.2018.01.029. URL http://www.sciencedirect.com/science/article/pii/S0896627318300540.

[10] Kevin C. Brennan, Luis Beltrn-Parrazal, Hector E. Lpez-Valds, Jeremy Theriot, Arthur W. Toga, and Andrew C. Charles. Distinct Vascular Conduction With Cortical Spreading Depression. *Journal of Neurophysiology*, 97(6):4143–4151, June 2007. ISSN 0022-3077, 1522-1598. doi: 10.1152/jn.00028.2007. URL http://www.physiology.org/doi/10.1152/jn.00028.2007.

[11] Susan Chalmers and David G. Nicholls. The Relationship between Free and Total Calcium Concentrations in the Matrix of Liver and Brain Mitochondria. *Journal of Biological Chemistry*, 278(21):19062–19070, May 2003. ISSN 0021-9258, 1083-351X. doi: 10.1074/jbc.M212661200. URL http://www.jbc.org/content/278/21/19062.

[12] Joshua C. Chang and Robert M. Miura. Regulatory inhibition of biological tissue mineralization by calcium phosphate through post-nucleation shielding by fetuin-A. *The Journal of Chemical Physics*, 144(15), April 2016. ISSN 0021-9606. doi: 10.1063/1.4946002. URL https://www.ncbi.nlm.nih.gov/pmc/articles/PMC4841804/.

[13] Joshua C. Chang, Lydia L. Shook, Jonathan Biag, Elaine N. Nguyen, Arthur W. Toga, Andrew C. Charles, and Kevin C. Brennan. Biphasic direct current shift, haemoglobin desaturation and neurovascular uncoupling in cortical spreading depression. *Brain*, 133(4):996–1012, April 2010. ISSN 0006-8950, 1460-2156. doi: 10.1093/brain/awp338. URL http://brain.oxfordjournals.org/content/133/4/996.

[14] Joshua C. Chang, Kevin C. Brennan, Dongdong He, Huaxiong Huang, Robert M. Miura, Phillip L. Wilson, and Jonathan J. Wylie. A Mathematical Model of the Metabolic and Perfusion Effects on Cortical Spreading Depression. *PLoS ONE*, 8(8):e70469, August 2013. doi: 10.1371/journal.pone.0070469. URL http://dx.doi.org/10.1371/journal.pone.0070469.

[15] A Charles and KC Brennan. Cortical spreading depressionnew insights and persistent questions. *Cephalalgia : an international journal of headache*, 29(10):1115–1124, October 2009. ISSN 0333-1024. doi: 10.1111/j.1468-2982.2009.01983.x. URL https://www.ncbi.nlm.nih.gov/pmc/articles/PMC5500297/.

[16] M. R. Christoffersen, J. Christoffersen, and W. Kibalczyc. Apparent solubilities of two amorphous calcium phosphates and of octacalcium phosphate in the temperature range 3042C. *Journal of Crystal Growth*, 106(2):349–354, November 1990. ISSN 0022-0248. doi: 10.1016/0022-0248(90)90079-Z. URL http://www.sciencedirect.com/science/article/pii/002202489090079Z.

[17] Julien Chuquet, Liad Hollender, and Esther A. Nimchinsky. High-Resolution In Vivo Imaging of the Neurovascular Unit during Spreading Depression. *Journal of Neuroscience*, 27(15):4036–4044, April 2007. ISSN 0270-6474, 1529-2401. doi: 10.1523/JNEUROSCI.0721-07.2007. URL http://www.jneurosci.org/content/27/15/4036.

[18] Nicolas Demaurex and Maud Frieden. Measurements of the free luminal ER Ca(2+) concentration with targeted "cameleon" fluorescent proteins. *Cell Calcium*, 34(2):109–119, August 2003. ISSN 0143-4160.

[19] S. S. Demir, J. W. Clark, C. R. Murphey, and W. R. Giles. A mathematical model of a rabbit sinoatrial node cell. *American Journal of Physiology-Cell Physiology*, 266(3): C832–C852, March 1994. ISSN 0363-6143. doi: 10.1152/ajpcell.1994.266.3.C832. URL https://www.physiology.org/doi/abs/10.1152/ajpcell.1994.266.3.C832.

[20] Archan Dey, Paul H. H. Bomans, Frank A. Mller, Julia Will, Peter M. Frederik, Gijsbertus de With, and Nico A. J. M. Sommerdijk. The role of prenucleation clusters in surface-induced calcium phosphate crystallization. *Nature Materials*, 9(12):1010–1014, December 2010. ISSN 1476-4660. doi: 10.1038/nmat2900. URL https://www.nature.com/articles/nmat2900.

[21] Katharina Dormanns, Richard George Brown, and Tim David. Neurovascular coupling: a parallel implementation. *Frontiers in Computational Neuroscience*, 9, 2015. ISSN 1662-5188. doi: 10.3389/fncom.2015.00109. URL https://www.frontiersin.org/articles/10.3389/fncom.2015.00109/full.

[22] Sergey V. Dorozhkin. Calcium orthophosphates: Occurrence, properties, biomineralization, pathological calcification and biomimetic applications. *Biomatter*, 1(2):121–164, October 2011. ISSN 2159-2535. doi: 10.4161/biom.18790. URL http://www.tandfonline.com/doi/abs/10.4161/biom.18790.

[23] JensP. Dreier and Clemens Reiffurth. The Stroke-Migraine Depolarization Continuum. *Neuron*, 86(4):902–922, May 2015. ISSN 0896-6273. doi: 10.1016/j.neuron.2015.04.004. URL http://www.sciencedirect.com/science/article/pii/S0896627315003335.

[24] Rune Enger, Wannan Tang, Gry Fluge Vindedal, Vidar Jensen, P. Johannes Helm, Rolf Sprengel, Loren L. Looger, and Erlend A. Nagelhus. Dynamics of Ionic Shifts in Cortical Spreading Depression. *Cerebral Cortex (New York, NY)*, 25(11):4469–4476, November 2015. ISSN 1047-3211. doi: 10.1093/cercor/bhv054. URL https://www.ncbi.nlm.nih.gov/pmc/articles/PMC4816793/.

[25] Hannah Farr and Tim David. Models of neurovascular coupling via potassium and EET signalling. *Journal of Theoretical Biology*, 286:13–23, October 2011. ISSN 0022-5193. doi: 10.1016/j.jtbi.2011.07.006. URL http://www.sciencedirect.com/science/article/pii/S002251931100350X.

[26] Denis Gebauer, Matthias Kellermeier, Julian D.Gale, Lennart Bergstrm, and Helmut Clfen. Pre-nucleation clusters as solute precursors in crystallisation. *Chemical Society Reviews*, 43(7):2348–2371, 2014. doi: 10.1039/C3CS60451A. URL https://pubs.rsc.org/en/content/articlelanding/2014/cs/c3cs60451a.

[27] Helene Girouard and Costantino Iadecola. Neurovascular coupling in the normal brain and in hypertension, stroke, and Alzheimer disease. *Journal of Applied Physiology*, 100 (1):328–335, January 2006. ISSN 8750-7587. doi: 10.1152/japplphysiol.00966.2005. URL https://www.physiology.org/doi/full/10.1152/japplphysiol.00966.2005.

[28] Helen M. Gniel and Rosemary L. Martin. Changes in Membrane Potential and the Intracellular Calcium Concentration During CSD and OGD in Layer V and Layer II/III Mouse Cortical Neurons. *Journal of Neurophysiology*, 104(6):3203–3212, December 2010. ISSN 0022-3077, 1522-1598. doi: 10.1152/jn.00922.2009. URL http://www.physiology.org/doi/10.1152/jn.00922.2009.

[29] Wouter J. E. M. Habraken, Jinhui Tao, Laura J. Brylka, Heiner Friedrich, Luca Bertinetti, Anna S. Schenk, Andreas Verch, Vladimir Dmitrovic, Paul H. H. Bomans, Peter M. Frederik, Jozua Laven, Paul van der Schoot, Barbara Aichmayer, Gijsbertus de With, James J. DeYoreo, and Nico A. J. M. Sommerdijk. Ion-association complexes unite classical and non-classical theories for the biomimetic nucleation of calcium phosphate. *Nature Communications*, 4:1507, February 2013. ISSN 2041-1723. doi: 10.1038/ncomms2490. URL https://www.nature.com/articles/ncomms2490.

[30] Jung Min Han, Akihiko Tanimura, Vivien Kirk, and James Sneyd. A mathematical model of calcium dynamics in HSY cells. *PLOS Computational Biology*, 13(2): e1005275, February 2017. ISSN 1553-7358. doi: 10.1371/journal.pcbi.1005275. URL https://journals.plos.org/ploscompbiol/article?id=10.1371/journal.pcbi.1005275.

[31] A. J. Hansen and C. E. Olsen. Brain extracellular space during spreading depression and ischemia. *Acta Physiologica Scandinavica*, 108(4):355–365, April 1980. ISSN 0001-6772. doi: 10.1111/j.1748-1716.1980.tb06544.x.

[32] Anker Jon Hansen and Thomas Zeuthen. Extracellular ion concentrations during spreading depression and ischemia in the rat brain cortex. *Acta Physiologica Scandinavica*, 113(4):437–445, December 1981. ISSN 00016772, 1365201X. doi: 10.1111/j.1748-1716.1981.tb06920.x. URL http://doi.wiley.com/10.1111/j.1748-1716.1981.tb06920.x.

[33] Margit Heiske, Thierry Letellier, and Edda Klipp. Comprehensive mathematical model of oxidative phosphorylation valid for physiological and pathological conditions. *The FEBS Journal*, 284(17):2802–2828, 2017. ISSN 1742-4658. doi: 10.1111/febs.14151. URL https://febs.onlinelibrary.wiley.com/doi/abs/10.1111/febs.14151.

[34] Alexander Heiss, Thomas Eckert, Anke Aretz, Walter Richtering, Wim van Dorp, Cora Schfer, and Willi Jahnen-Dechent. Hierarchical Role of Fetuin-A and Acidic Serum Proteins in the Formation and Stabilization of Calcium Phosphate Particles. *Journal of Biological Chemistry*, 283(21):14815–14825, May 2008. ISSN 0021-9258, 1083-351X. doi: 10.1074/jbc.M709938200. URL http://www.jbc.org/content/283/21/14815.

[35] Alexander Heiss, Vitaliy Pipich, Willi Jahnen-Dechent, and Dietmar Schwahn. Fetuin-A Is a Mineral Carrier Protein: Small Angle Neutron Scattering Provides New Insight on Fetuin-A Controlled Calcification Inhibition. *Biophysical Journal*, 99(12):3986–3995, December 2010. ISSN 0006-3495. doi: 10.1016/j.bpj.2010.10.030. URL http://www.ncbi.nlm.nih.gov/pmc/articles/PMC3000477/.

[36] Erin R. Higgins, Mark B. Cannell, and James Sneyd. A Buffering SERCA Pump in Models of Calcium Dynamics. *Biophysical Journal*, 91(1):151–163, July 2006. ISSN 0006-3495. doi: 10.1529/biophysj.105.075747. URL https://www.ncbi.nlm.nih.gov/pmc/articles/PMC1479058/.

[37] David C. Hill-Eubanks, Matthias E. Werner, Thomas J. Heppner, and Mark T. Nelson. Calcium Signaling in Smooth Muscle. *Cold Spring Harbor Perspectives in Biology*, 3(9), September 2011. ISSN 1943-0264. doi: 10.1101/cshperspect.a004549. URL https://www.ncbi.nlm.nih.gov/pmc/articles/PMC3181028/.

[38] Willi Jahnen-Dechent, Alexander Heiss, Cora Schfer, and Markus Ketteler. Fetuin-A Regulation of Calcified Matrix Metabolism. *Circulation Research*, 108(12):1494–1509, June 2011. ISSN 0009-7330, 1524-4571. doi: 10.1161/CIRCRESAHA.110.234260. URL http://circres.ahajournals.org/content/108/12/1494.

[39] Jaijus Pallippadan Johny, Michael J. Plank, and Tim David. Importance of Altered Levels of SERCA, IP3r, and RyR in Vascular Smooth Muscle Cell. *Biophysical Journal*, 112(2):265–287, January 2017. ISSN 0006-3495. doi: 10.1016/j.bpj.2016.11.3206. URL http://www.sciencedirect.com/science/article/pii/S0006349516342795.

[40] Adam Kapela, Anastasios Bezerianos, and Nikolaos M. Tsoukias. A mathematical model of Ca2+ dynamics in rat mesenteric smooth muscle cell: Agonist and NO stimulation. *Journal of Theoretical Biology*, 253(2):238–260, July 2008. ISSN 0022-5193. doi: 10.1016/j.jtbi.2008.03.004. URL http://www.sciencedirect.com/science/article/pii/S0022519308001173.

[41] Dan Kaufmann, Jeremy J Theriot, Jekaterina Zyuzin, C Austin Service, Joshua C Chang, Y Tanye Tang, Vladimir B Bogdanov, Sylvie Multon, Jean Schoenen, Y Sungtaek Ju, and KC Brennan. Heterogeneous incidence and propagation of spreading depolarizations. *Journal of Cerebral Blood Flow & Metabolism*, 37(5):1748–1762, May 2017. ISSN 0271-678X. doi: 10.1177/0271678X16659496. URL https://doi.org/10.1177/0271678X16659496.

[42] Tatiana Kulakovskaya, Evgeny Pavlov, and Elena N. Dedkova, editors. *Inorganic Polyphosphates in Eukaryotic Cells*. Springer International Publishing, 2016. ISBN 978-3-319-41071-5. URL https://www.springer.com/gp/book/9783319410715.

[43] Martin Lauritzen. Long-Lasting Reduction of Cortical Blood Flow of the Rat Brain after Spreading Depression with Preserved Autoregulation and Impaired CO2 Response. *Journal of Cerebral Blood Flow & Metabolism*, 4(4):546–554, December 1984. ISSN 0271-678X. doi: 10.1038/jcbfm.1984.79. URL https://doi.org/10.1038/jcbfm.1984.79.

[44] Martin Lauritzen. Pathophysiology of the migraine auraThe spreading depression theory. *Brain*, 117(1):199–210, February 1994. ISSN 0006-8950. doi: 10.1093/brain/117.1.199. URL https://academic.oup.com/brain/article/117/1/199/373383.

[45] Martin Lauritzen, Jens Peter Dreier, Martin Fabricius, Jed A Hartings, Rudolf Graf, and Anthony John Strong. Clinical relevance of cortical spreading depression in neurological disorders: migraine, malignant stroke, subarachnoid and intracranial hemorrhage, and traumatic brain injury. *Journal of Cerebral Blood Flow & Metabolism*, 31(1):17–35, January 2011. ISSN 0271-678X. doi: 10.1038/jcbfm.2010.191. URL https://www.ncbi.nlm.nih.gov/pmc/articles/PMC3049472/.

[46] Aristides A. P. Leao. Spreading depression of activity in the cerebral cortex. *Journal of Neurophysiology*, 7(6):359–390, November 1944. ISSN 0022-3077. doi: 10.1152/jn.1944.7.6.359. URL https://www.physiology.org/doi/abs/10.1152/jn.1944.7.6.359.

[47] G. Lemon, W. G. Gibson, and M. R. Bennett. Metabotropic receptor activation, desensitization and sequestrationI: modelling calcium and inositol 1,4,5-trisphosphate dynamics following receptor activation. *Journal of Theoretical Biology*, 223(1):93–111, July 2003. ISSN 0022-5193. doi: 10.1016/S0022-5193(03)00079-1. URL http://www.sciencedirect.com/science/article/pii/S0022519303000791.

[48] Gerhard Magnus and Joel Keizer. Model of -cell mitochondrial calcium handling and electrical activity. II. Mitochondrial variables. *American Journal of Physiology-Cell Physiology*, 274 (4):C1174–C1184, April 1998. ISSN 0363-6143. doi: 10.1152/ajpcell.1998.274.4.C1174. URL https://www.physiology.org/doi/full/10.1152/ajpcell.1998.274.4.C1174.

[49] Shawn Means, Alexander J. Smith, Jason Shepherd, John Shadid, John Fowler, Richard J. H. Wojcikiewicz, Tomas Mazel, Gregory D. Smith, and Bridget S. Wilson. Reaction Diffusion Modeling of Calcium Dynamics with Realistic ER Geometry. *Biophysical Journal*, 91(2):537–557, July 2006. ISSN 0006-3495. doi: 10.1529/biophysj.105.075036. URL https://www.ncbi.nlm.nih.gov/pmc/articles/PMC1483115/.

[50] Robert M. Miura, Huaxiong Huang, and Jonathan J. Wylie. Mathematical approaches to modeling of cortical spreading depression. *Chaos: An Interdisciplinary Journal of Nonlinear Science*, 23(4):046103, December 2013. ISSN 1054-1500, 1089-7682. doi: 10.1063/1.4821955. URL http://aip.scitation.org/doi/10.1063/1.4821955.

[51] Charles Nicholson, Kevin C. Chen, Sabina Hrabtov, and Lian Tao. Diffusion of molecules in brain extracellular space: theory and experiment. In *Progress in Brain Research*, volume 125 of *Volume Transmission Revisited*, pages 129–154. Elsevier, January 2000. doi: 10.1016/S0079-6123(00)25007-3. URL http://www.sciencedirect.com/science/article/pii/S0079612300250073.

[52] Daniela Pietrobon and Michael A. Moskowitz. Chaos and commotion in the wake of cortical spreading depression and spreading depolarizations. *Nature Reviews Neuroscience*, 15(6):379–393, June 2014. ISSN 1471-0048. doi: 10.1038/nrn3770. URL https://www.nature.com/articles/nrn3770.

[53] Henning Piilgaard and Martin Lauritzen. Persistent Increase in Oxygen Consumption and Impaired Neurovascular Coupling after Spreading Depression in Rat Neocortex. *Journal of Cerebral Blood Flow & Metabolism*, 29(9):1517–1527, September 2009. ISSN 0271-678X. doi: 10.1038/jcbfm.2009.73. URL https://doi.org/10.1038/jcbfm.2009.73.

[54] Henning Piilgaard, Brent M Witgen, Peter Rasmussen, and Martin Lauritzen. Cyclosporine A, FK506, and NIM811 ameliorate prolonged CBF reduction and impaired neurovascular coupling after cortical spreading depression. *Journal of Cerebral Blood Flow & Metabolism*, 31(7):1588–1598, July 2011. ISSN 0271-678X, 1559-7016. doi: 10.1038/jcbfm.2011.28. URL http://journals.sagepub.com/doi/10.1038/jcbfm.2011.28.

[55] Anna Maria Porcelli, Anna Ghelli, Claudia Zanna, Paolo Pinton, Rosario Rizzuto, and Michela Rugolo. pH difference across the outer mitochondrial membrane measured with a green fluorescent protein mutant. *Biochemical and Biophysical Research Communications*, 326(4):799–804, January 2005. ISSN 0006-291X. doi: 10.1016/j.bbrc.2004.11.105.

[56] Aaron S. Posner and Foster Betts. Synthetic amorphous calcium phosphate and its relation to bone mineral structure. *Accounts of Chemical Research*, 8(8):273–281, August 1975. ISSN 0001-4842. doi: 10.1021/ar50092a003. URL http://dx.doi.org/10.1021/ar50092a003.

[57] Christopher Rackauckas and Qing Nie. DifferentialEquations.jl A Performant and Feature-Rich Ecosystem for Solving Differential Equations in Julia. *Journal of Open Research Software*, 5(1):15, May 2017. ISSN 2049-9647. doi: 10.5334/jors.151. URL http://openresearchsoftware.metajnl.com/articles/10.5334/jors.151/.

[58] P. M. Sawant-Pokam, P. Suryavanshi, J. M. Mendez, F. E. Dudek, and K. C. Brennan. Mechanisms of Neuronal Silencing After Cortical Spreading Depression. *Cerebral Cortex*, 27(2), January 2016. ISSN 1460-2199, 1047-3211. doi: 10.1093/cercor/bhv328. URL https://academic.oup.com/cercor/article/doi/10.1093/cercor/bhv328/3056266.

[59] Maria E. Solesio, Luis C. Garcia del Molino, Pia A. Elustondo, Diao Catherine, Joshua C. Chang, and Evgeny V. Pavlov. Inorganic polyphosphate (polyP) is required for sustained free mitochondrial calcium elevation, following stimulated calcium uptake. *bioRxiv*, page 493825, December 2018. doi: 10.1101/493825. URL https://www.biorxiv.org/content/10.1101/493825v1.

[60] D. Swaminathan, G. Ullah, and P. Jung. A simple sequential-binding model for calcium puffs. *Chaos: An Interdisciplinary Journal of Nonlinear Science*, 19(3):037109, September 2009. ISSN 1054-1500. doi: 10.1063/1.3152227. URL https://aip.scitation.org/doi/10.1063/1.3152227.

[61] Eva Sykov and Charles Nicholson. Diffusion in Brain Extracellular Space. *Physiological reviews*, 88(4):1277–1340, October 2008. ISSN 0031-9333. doi: 10.1152/physrev.00027.2007. URL https://www.ncbi.nlm.nih.gov/pmc/articles/PMC2785730/.

[62] Takahiro Takano, Guo-Feng Tian, Weiguo Peng, Nanhong Lou, Ditte Lovatt, Anker J Hansen, Karl A Kasischke, and Maiken Nedergaard. Cortical spreading depression causes and coincides with tissue hypoxia. *Nature Neuroscience*, 10(6):754–762, June 2007. ISSN 1097-6256, 1546-1726. doi: 10.1038/nn1902. URL http://www.nature.com/articles/nn1902.

[63] B. J. Tarasevich, C. C. Chusuei, and D. L. Allara. Nucleation and Growth of Calcium Phosphate from Physiological Solutions onto Self-Assembled Templates by a Solution-Formed Nucleus Mechanism. *The Journal of Physical Chemistry B*, 107(38):10367–10377, September 2003. ISSN 1520-6106. doi: 10.1021/jp027445p. URL http://dx.doi.org/10.1021/jp027445p.

[64] Jeremy J. Theriot, Arthur W. Toga, Neal Prakash, Y. Sungtaek Ju, and K. C. Brennan. Cortical Sensory Plasticity in a Model of Migraine with Aura. *Journal of Neuroscience*, 32(44):15252–15261, October 2012. ISSN 0270-6474, 1529-2401. doi: 10.1523/JNEUROSCI.2092-12.2012. URL https://www.jneurosci.org/content/32/44/15252.

[65] Benjamin Wacquier, Laurent Combettes, Guy Tran Van Nhieu, and Genevive Dupont. Interplay Between Intracellular Ca^{2+} Oscillations and Ca^{2+}-stimulated Mitochondrial Metabolism. *Scientific Reports*, 6:19316, January 2016. doi: 10.1038/srep19316. URL https://www.nature.com/articles/srep19316.

[66] Benjamin Wacquier, Hugo E. Romero Campos, Virginia GonzlezVlez, Laurent Combettes, and Genevive Dupont. Mitochondrial Ca2+ dynamics in cells and suspensions. *The FEBS Journal*, 284(23):4128–4142, 2017. ISSN 1742-4658. doi: 10.1111/febs.14296. URL https://febs.onlinelibrary.wiley.com/doi/abs/10.1111/febs.14296.

[67] J Wagner and J Keizer. Effects of rapid buffers on Ca2+ diffusion and Ca2+ oscillations. *Biophysical Journal*, 67 (1):447–456, July 1994. ISSN 0006-3495. URL https://www.ncbi.nlm.nih.gov/pmc/articles/PMC1225377/.

[68] Lijun Wang and George H. Nancollas. Calcium Orthophosphates: Crystallization and Dissolution. *Chemical reviews*, 108(11):4628–4669, November 2008. ISSN 0009-2665. doi: 10.1021/cr0782574. URL http://www.ncbi.nlm.nih.gov/pmc/articles/PMC2743557/.

[69] George S. B. Williams, Liron Boyman, Aristide C. Chikando, Ramzi J. Khairallah, and W. J. Lederer. Mitochondrial calcium uptake. *Proceedings of the National Academy of Sciences*, 110(26):10479–10486, June 2013. ISSN 0027-8424, 1091-6490. doi: 10.1073/pnas.1300410110. URL https://www.pnas.org/content/110/26/10479.

[70] Hsueh Yang, Gabrielle Curinga, and Cecilia M. Giachelli. Elevated extracellular calcium levels induce smooth muscle cell matrix mineralization in vitro. *Kidney International*, 66(6): 2293–2299, December 2004. ISSN 00852538. doi: 10.1111/j.1523-1755.2004.66015.x. URL https://linkinghub.elsevier.com/retrieve/pii/S0085253815503335.

[71] Jin Yang, John W. Clark, Robert M. Bryan, and Claudia Robertson. The myogenic response in isolated rat cerebrovascular arteries: smooth muscle cell model. *Medical Engineering & Physics*, 25(8):691–709, October 2003. ISSN 1350-4533. doi: 10.1016/S1350-4533(03)00100-0. URL http://www.sciencedirect.com/science/article/pii/S1350453303001000.

[72] Xilin Yin and Malcolm J. Stott. Biological calcium phosphates and Posners cluster. *The Journal of Chemical Physics*, 118(8):3717–3723, February 2003. ISSN 0021-9606, 1089-7690. doi: 10.1063/1.1539093. URL http://scitation.aip.org/content/aip/journal/jcp/118/8/10.1063/1.1539093.

[73] Bas-Jan Zandt, Haken Bennie ten, Putten Michel J.A.M. van, and Markus A. Dahlem. How does spreading depression spread? Physiology and modeling. *Reviews in the Neurosciences*, 26(2):183–198, 2015. ISSN 2191-0200. doi: 10.1515/revneuro-2014-0069. URL https://www.degruyter.com/view/j/revneuro.2015.26.issue-2/revneuro-2014-0069/revneuro-2014-0069.xml.